

Integrated petrophysical evaluation and rock physics modelling of LBS sands in the Kuargaon Field, Assam and Assam-Arakan Basin, India

Jayendra Nath Chakraborty¹, Manoj Kumar¹, Debashree Paul¹, and Sunil Kumar Singh¹

ABSTRACT

Rock physics serves as a bridge connecting different disciplines of exploration geosciences providing key insights to understand complex information embedded within the subsurface data. Seismic reservoir characterization studies often face challenges in the form of absence or suboptimal quality of acoustic (P-wave) and shear sonic (S-wave) logs, which can be derived from iterative petrophysics and rock physics modelling. In this study, we present a robust methodology to model both primary (P-wave) and shear (Swave) velocities in the Oligocene deltaic Barail Coal Shale (BCS) sequence of the Upper Assam North Shelf. This formation is characterized by thin sand layers, referred to as Lakhwa Barail Sands (LBS), interbedded with coal, shale, and carbonaceous shale, making accurate velocity estimation difficult—especially in intervals affected by borehole rugosity, where density logs often become unreliable. For addressing such complexities, we performed a comprehensive formation evaluation by integrating log, core, and geological data. Density logs were conditioned using Multi-Resolution Graph-Based Clustering (MRGC), with NPHI, DT, RT, and GR logs as inputs in intervals with good borehole conditions. A petrophysical model was developed using Routine Core Analysis (RCAL) and Special Core Analysis (SCAL) data, enabling the generation of sand-shale volume fractions. Elastic properties were modelled using the effective medium theory and were calibrated with core-derived elastic moduli measured near reservoir pressure. The resulting workflow demonstrated a reliable approach to lithofacies discrimination in the elastic domain and can be applied to other geologically similar settings.

KEYWORDS

Rock physics, aspect ratio, elastic modulus, reservoir characterization, petrophysical modeling

INTRODUCTION

This study focuses on the petrophysical formation evaluation and rock physics modelling of the Oligocene Barail Coal Shale (BCS) interval within selected wells from the Kuargaon (main field) and nearby Lakwa_Lakhmani, Demulgaon, as well as Mahakuti fields in the Upper Assam North Shelf, India (Figure 1a). The regional

stratigraphy comprises a Precambrian granite-gneissic basement overlain by Paleogene sedimentary sequences, including the Basal Tura Sand, Sylhet Limestone, Kopili Shale, and the coal-shale-sand assemblage of the Barail Group (Figure 1b). The Barail Group is further subdivided into the Demulgaon and Dishangmukh formations representing delta-front sandstone successions (Barail Main Sand, BMS)—followed by the Rudrasagar Formation, characterized by delta-plain sands interbedded with coal and shale, known as the Barail Coal Shale (BCS), as stated above. The BCS is predominantly composed of coal and shale, with isolated sandstone bodies. referred to as Lakhwa Barail Sands (LBS). These LBS units act as significant hydrocarbon reservoirs in the region. However, their lateral heterogeneity and variable thickness across wells considerable introduce challenges in reservoir delineation and development planning.

AVAILABLE DATA

Twelve wells were selected for this study based on their regional distribution over the study area (Figure 2). Of these, seven wells had shear sonic logs were available within the depth interval of interest. Additionally, laboratory-derived petrophysical parameters and elastic properties from a conventional core sample targeting the BCS section were integrated into the analysis. The findings from these seven wells with reliable shear data are frequently referenced throughout the study due to their superior data integrity.

METHODOLOGY

The study was carried out in several steps. It began with the analysis of the recorded well data, including log conditioning, depth matching, curve editing, and synthetic log reconstruction using the Multi-Resolution Graph-Based Clustering (MRGC) technique. Advanced sonic data were reprocessed, where necessary, to improve shear wave data quality. Once the data were properly conditioned, petrophysical parameters were estimated and validated against RCAL and SCAL data to

¹INTEG, GEOPIC, ONGC, Dehradun, India

Emails: chakraborty jayendra@ongc.co.in; kumar manoj7@ongc.co.in; paul bebashree@ongc.co.in; singh sunilkumar@ongc.co.in

ensure a near consistent field-wide petrophysical model. The estimated petrophysical parameters included volume of shale, total and effective porosity, and water saturation, with calculation methods detailed in Appendix A (Azeem et al., 2017)., Following the

computation of calibrated petrophysical parameters, rock physics modelling was carried out (post rock physics diagnostics) using computed mineral and fluid volumes and pore aspect ratios, guided qualitatively by petrographic observations about the pore size (Figure-7a

Barbill Saronal Disamman Jordan Samdang Disamman Pengrapan Disamman Jordan Dechal Languaga Bogapa DIGBOI Khe Rajali MAHORKATIVA Kusijan Khu Mahaman Jordan Baranaga THU Kusijan Khu Mahaman Jordan Baranaga THU Kusijan Lakhanaji Nahorhat Lakhan

and b) from core samples. Model outputs iteratively refined to achieve a satisfactory match between recorded and simulated Pand S-wave velocities, P and S impedance logs, V_P/V_S ratio, and elastic moduli. Final of calibration elastic used coreparameters derived moduli, computed at approximately 4000 psi to reflect near-reservoir The conditions. pressure generalized workflow followed is shown in Figure 3.

(b)

AGE	FORMATION / SAND		LITHOLOG	GROSS LITHOLOGY					
ne .									
Miocene	ř.	LCM+TS4	response production for	Dominantly clay/ claystone with occasional sand sandstones					
	Galeki Sst.	TS-5		Intercalation of sand /sandstone with clay /clayston and siltstone.					
	Š	TS-6		and sittstone.					
Oligocene	Barails	Rudrasagar (BCS)		Dominantly shale inter-bedded with coal and minor cla stone with Sand and siltstone					
Oligo		Demulgaon (BMS)		Dominantly fine to medium grained grey sandstone with some inter-bedded clay and shale.					
Late Eocene		Kopili		Mainly shale (splintery) alternating with fine grained sandstone and siltstone.					
Middle Eocene		Sylhet		Mainly fossiliferous limestone with shales and this sandstone bands.					

Figure 1: (a) Location map of the study area (adapted from Chakrabarty et al., 2022). (b) Stratigraphy of Upper Assam North Area

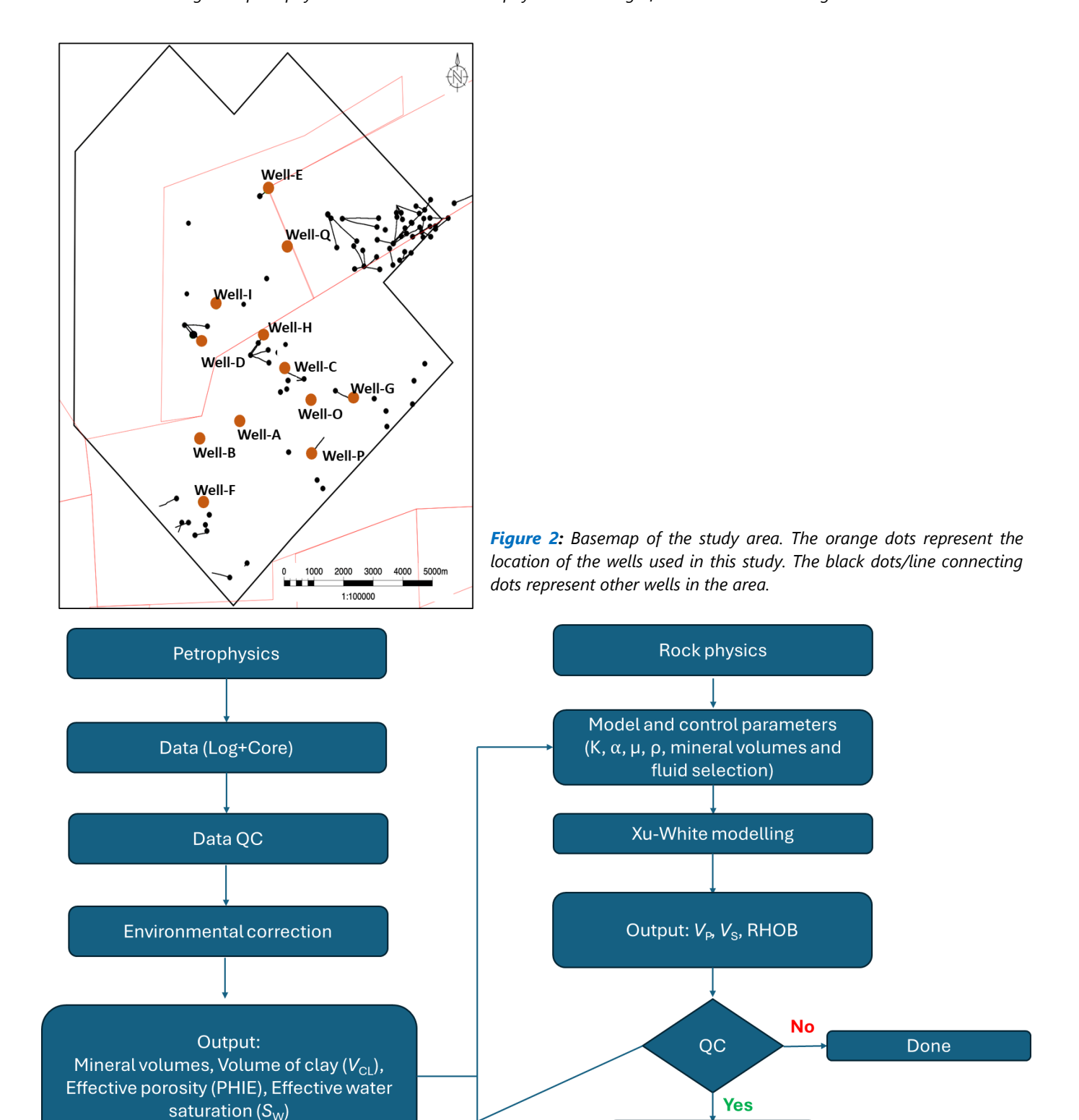


Figure 3: The generic rock physics modelling workflow followed for the study.

Done

ADVANCED SONIC LOG PROCESSING

Semblance processing was applied to generate highquality compressional and shear slowness curves. In four selected wells, advanced sonic data were further refined through manual interpretation. Automated semblance picking algorithms often yield unexpected results in lithologies dominated by coal, shales, or other highly attenuative formations. To address this limitation, monopole and dipole waveforms were manually interpreted to reduce the uncertainties associated with

auto-picked shear slowness curves. The resulting manually picked curves were geologically consistent and honoured the petrophysical log responses. A comparative analysis between the auto-picked and manually interpreted curves revealed (Figure 4a-b) significant improvements in accuracy and reliability. These refined curves served as the basis for generating synthetic shear logs in wells lacking reliable shear data.

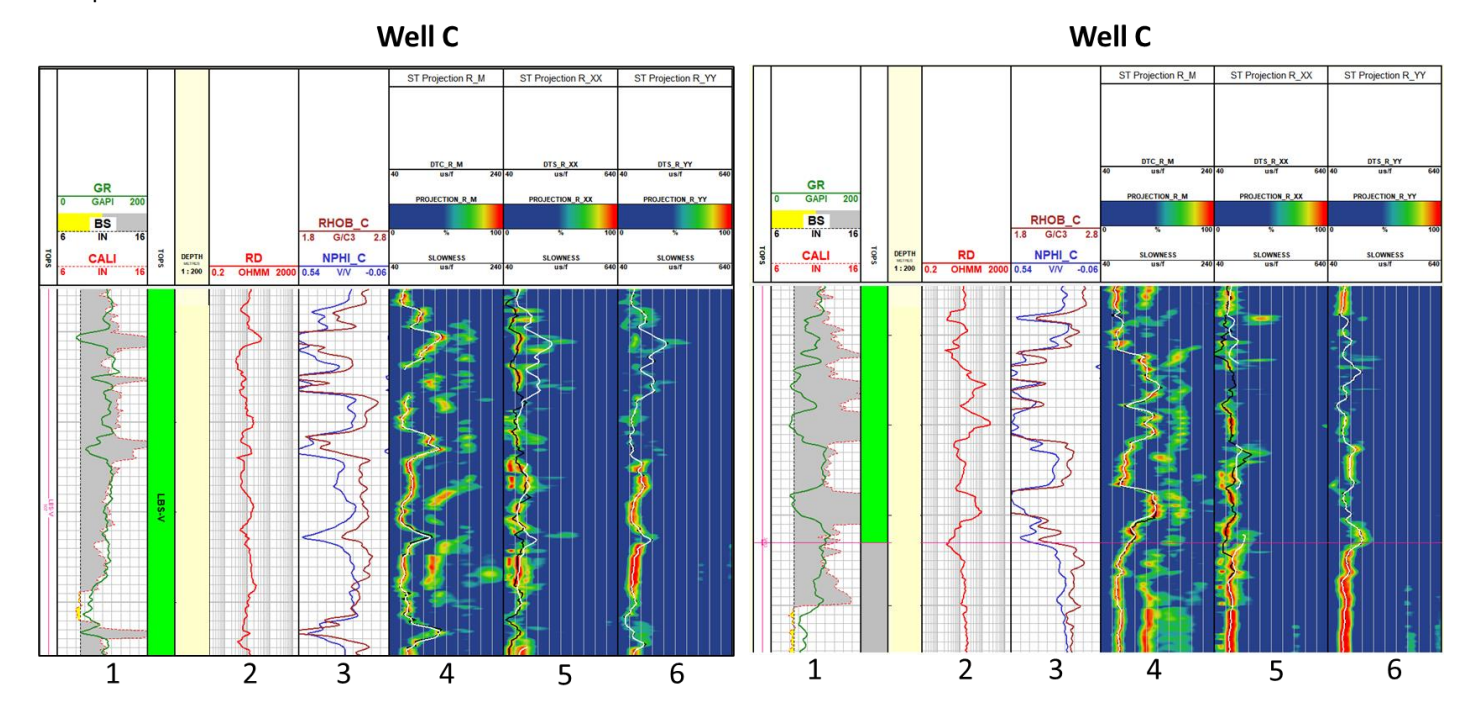


Figure 4: Examples of advanced sonic processing. Tracks 1–3 display basic petrophysical logs (e.g., gamma ray (GR), density (RHOB) and neutron porosity (NPHI)). Auto-picked (black) and manually interpreted (white) shear slowness curves are shown in Track 4 (monopole waveform) and Track 5-6 (dipole waveforms). Manual interpretation demonstrates improved alignment with geological and petrophysical features, particularly in coal and shaly intervals.

SYNTHETIC SHEAR LOG GENERATION

The workflow involved application of multilinear modelling, leveraging regression core-calibrated volumetric data obtained during petrophysical analysis. Five representative wells were selected based on their spatial distribution and data quality, and they served as the basis for model development. A robust petrophysical model was initially constructed using RCAL and SCAL data for calibration. The resulting mineral volumes and recorded basic logs—including P-velocity (V_P), neutron porosity (NPHI), density (RHOB), and gamma ray (GR)—

were used to derive synthetic shear wave velocity (V_s) logs (equation1). The generation process for these synthetic logs was then extended to other wells across the field that either lacked recorded shear data or contained unreliable shear logs due to poor borehole conditions (e.g., rugosity or washouts). This empirical approach ensured that shear velocity predictions were consistent with both petrophysical, and geological trends observed in the core-calibrated reference wells.

 $V_S = 2261.6 + 0.48* V_P - 3947.5*NPHI + 485.4*RHOB - 1357*QUARTZ - 2.75*GR - 1523.6*CLAY - 0.88*RD - 978.2*SM1, (1)$

where RD is deep resistivity (in ohm-m), and SM1 represents volume of a special mineral.

The recorded P-velocity and the computed S-velocity measured in ft/s were subsequently cross-plotted for each reservoir zone to establish zone-specific linear regression relationships as shown in Figure 5. These equations can be applied to other wells across the field where only sonic log data are available, thereby enabling generation of S-velocity logs in the absence of direct measurements which can at least serve as a guide or give some idea about the velocity variations across the lithologies, provided there is no abrupt change in the geology represented by localized over pressured zones or severe compartmentalization leading to structural uncertainties which may have sands deposited in different pressure regimes.

BCS : $-673.5 + 0.57* V_P$ (2) LBS-VI : $-1206.6 + 0.62* V_P$ (3) LBS-V : $-726.5 + 0.60* V_P$ (4) LBS-IV : $-746.6 + 0.58* V_P$ (5) LBS-II : $-516.8 + 0.61* V_P$ (6)

(All these equations have a correlation coefficient of more than 0.79)

A final composite shear velocity log was constructed by splicing the high-quality shear slowness data obtained from advanced sonic processing in wells with good borehole conditions with the synthetic shear log generated using the multilinear regression model. This hybrid log provided a consistent and geologically valid shear velocity profile, serving as a crucial input for subsequent rock physics modelling.

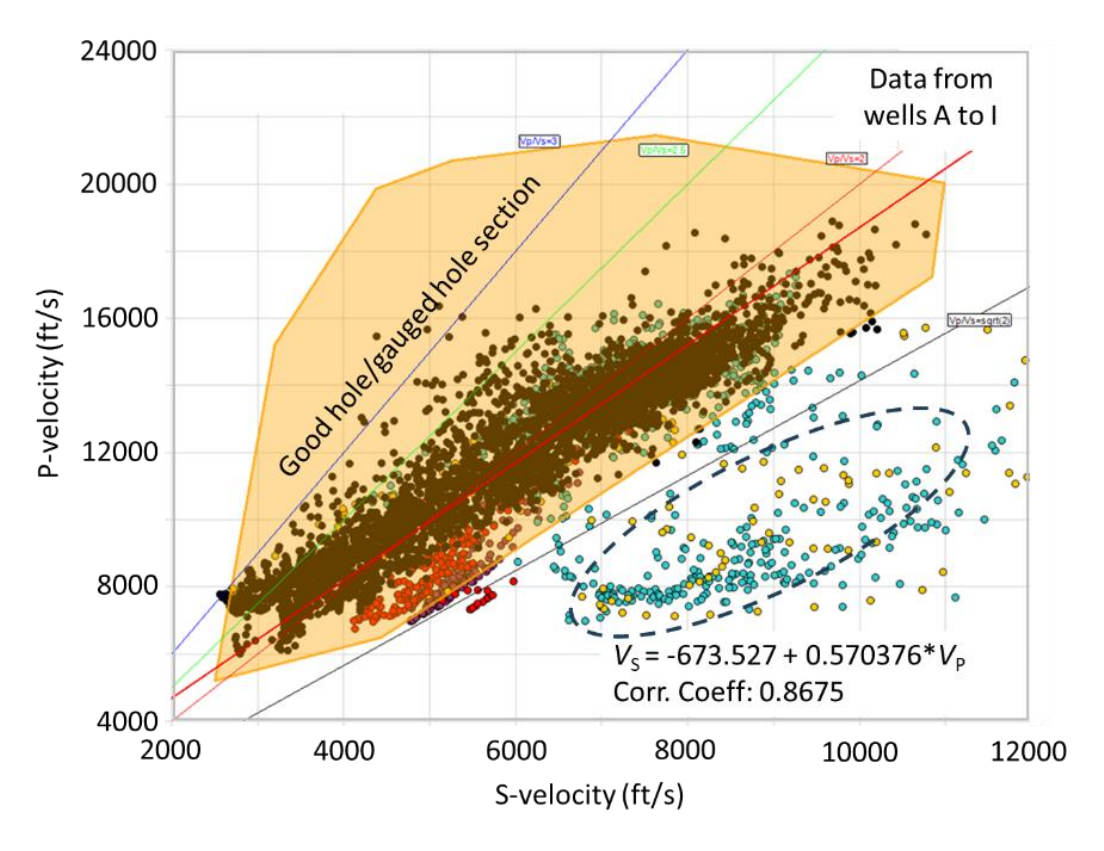


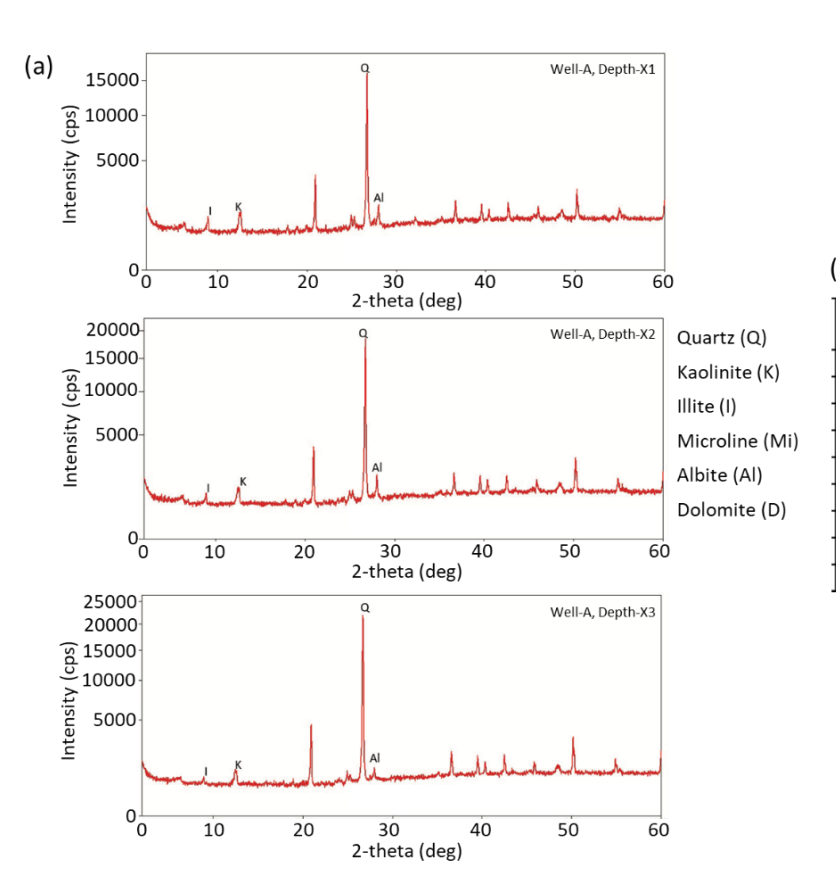
Figure-5: Crossplot between P-velocity (V_P) and S-velocity (V_S) for wells A through I within the BCS section. The data points seen enclosed by the dashed black polygon are interpreted as affected by bad borehole/rugose hole conditions.

PETROPHYSICAL EVALUATION

Petrophysical performed evaluation was foundational step to quantify key reservoir parameters, including volume of clay, porosity, and water saturation. The quality of log data and accuracy in volumetric estimation directly influence the reliability of subsequent rock physics modelling (Avseth et al., 2001). A suite of conventional well logs—gamma ray (GR), bulk density (RHOB), neutron porosity (NPHI), resistivity (RT), and compressional slowness (DT)—was employed to derive volume of clay, porosity and water saturation. The detailed methodology and associated equations are provided in Appendix A. The computed petrophysical results were rigorously calibrated against routine core analysis (RCAL) data to ensure consistency and reliability.

Petrophysical model

The petrophysical model was developed using inputs from density versus neutron porosity cross plots, X-ray diffraction (XRD) analysis, and core-derived mineralogical data. Based on this integrated interpretation, quartz was selected as the dominant framework mineral due to its prevalence and stability in the BCS sandstones. A single representative clay type was incorporated into the model, with endmember properties closely approximating kaolinite, based on petrographic and XRD indicators (Figures 6a and b). Additionally, a mixed silicate component comprising feldspar was included and is denoted as SM1 in this study. The formation water resistivity $(R_{\rm W})$ used in the water-saturation calculations was derived from produced water salinity as well as Pickett Plot analysis (Table-1) and regional salinity data, ensuring that the model reflects true *in-situ* conditions.



	١.
h	1
v	,

Montmorillonite/	Illite	Kaolinite	Quartz	Microcline	Albite	Dolomite	Siderite
Chlorite (%)	(%)	(%)	(%)	(%)	(%)	(%)	(%)
	Tr.	6.3	84.53		9.16		
	Tr.	6.27	86.34		7.4		
	5.41	7.29	78.22		9.08		
	Tr.	5.84	86.24		7.92		
	Tr.	Tr.	89.89		5.2		
	7.81	8.25	74.53		9.41		
	10.06	10.58	65.84		13.52		
	8.62	9.41	69.02		12.94		
	8.37	9.31	59.78		10.91		11.63

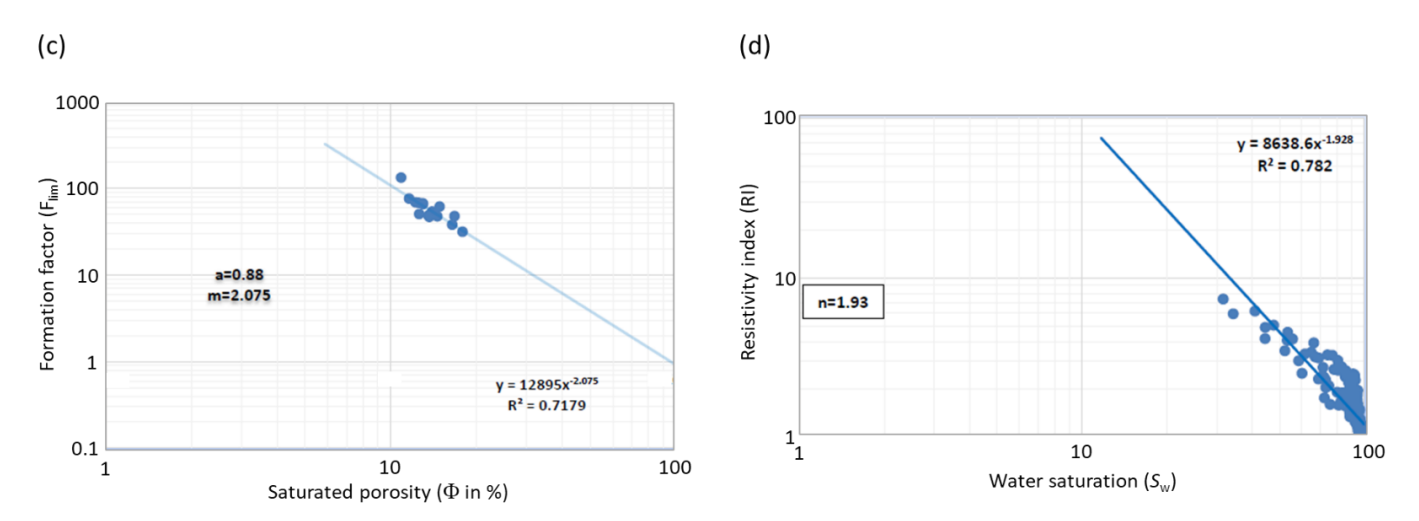


Figure 6: (a) XRD analysis of core samples (within LBS sands), and (b) XRD bulk data of plug samples of LBS sands. Crossplots between (c) saturated porosity (F) and Formation Factor (F_{lim}), and (d) Water saturation (S_w) and Resistivity Index (RI) for LBS sands.

Table-1: Resistivity of Formation Water (Pickett Plot Analysis)

S. No.	Formation/pays	Rw (ohm-m)
1	LBS	0.25-0.30 ohmm@90 degC (~7-9gpl)
2	BMS	0.25-0.30 ohmm@90 degC (~7-9gpl)

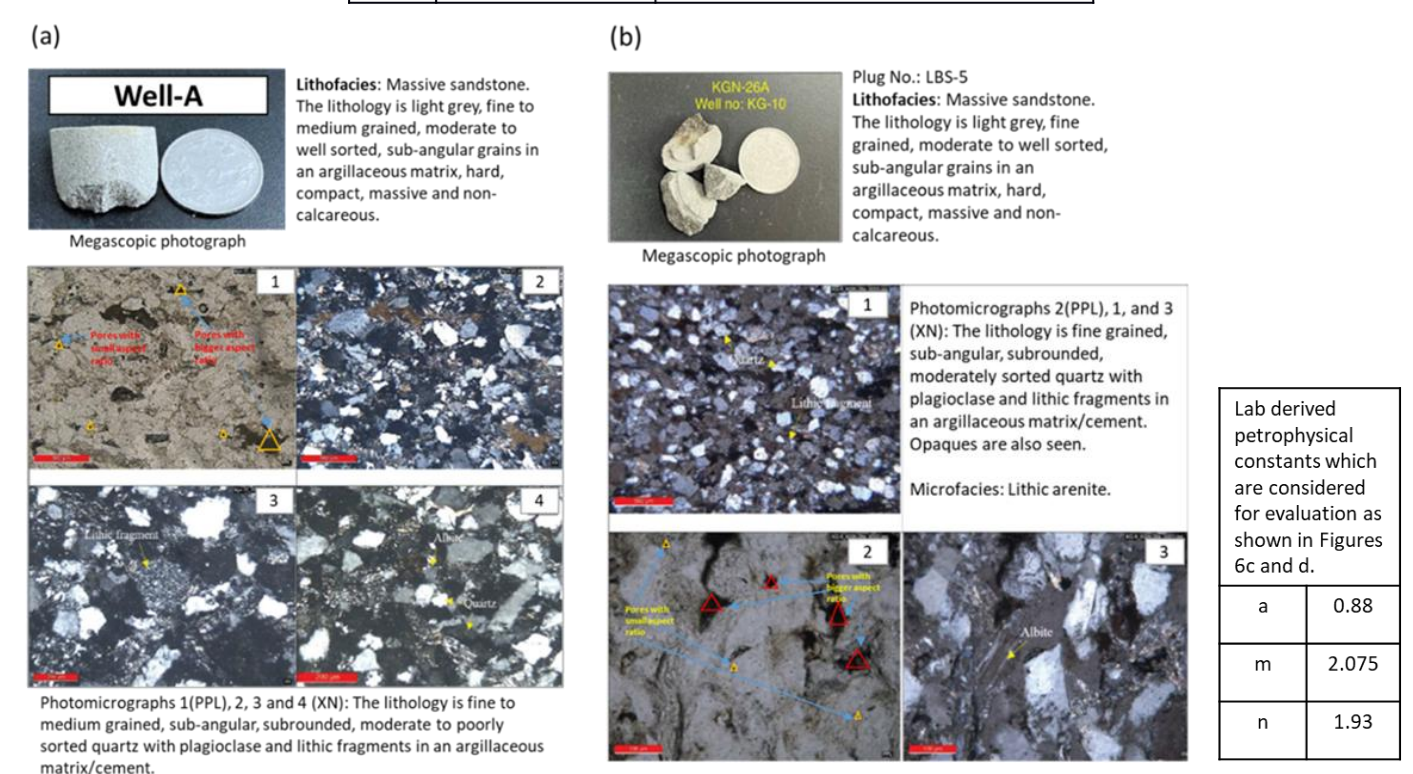


Figure 7: Core megascopic study and petrographic samples (CC-1 against LBS sand in Well-A) (CC-1 represents the first conventional core taken in well-A)

Microfacies: Lithic arenite.

Table-2: Petrophysical properties of the core plugs

S. No	Plug No.	Well no.	Depth (m)	Porosity (%)	K (he) (mD)	Grain density (g/cm³)	Bulk density (g/cm³)
30	CP-1	А	X1	11.705	1.780	2.645	2.335
31	CP-2	А	X2	12.353	2.543	2.658	2.330
32	CP-3A	А	Х3	10.278	1.013	2.648	2.376
33	CP-3B	Α	Х3	10.612	0.827	2.674	2.390
34	CP-4A	Α	X4	10.486	1.219	2.645	2.367
35	CP-4B	А	X4	10.680	1.124	2.651	2.368
36	CP-5A	А	X5	13.239	5.211	2.643	2.293
37	CP-5B	А	X5	13.447	6.185	2.640	2.285
38	CP-6A	А	Х6	10.088	1.263	2.656	2.388
39	CP-6B	Α	Х6	10.127	0.727	2.668	2.398
40	CP-7	А	X7	11.892	1.638	2.676	2.358
41	CP-8A	Α	X8	12.373	1.912	2.663	2.333
42	CP-8B	А	X8	12.938	1.952	2.664	2.319
43	CP-9A	Α	Х9	13.245	3.354	2.651	2.300
44	CP-9B	А	X9	12.540	2.661	2.637	2.306
45	CP-10A	Α	X10	16.093	15.968	2.657	2.229
46	CP-10B	Α	X10	15.943	18.784	2.653	2.230
47	CP-11A	Α	X11	14.164	4.665	2.669	2.291
48	CP-11B	Α	X11	13.961	4.366	2.672	2.299
49	CP-12A	Α	X12	18.059	57.949	2.655	2.176
50	CP-12B	А	X12	18.594	56.364	2.655	2.161
51	CP-13A	А	X13	13.534	3.332	2.640	2.283
52	CP-13B	Α	X13	13.688	2.967	2.665	2.300
53	CP-15A	Α	X14	3.394	0.044	2.764	2.671
54	CP-15B	A	X14	3.514	0.681	2.763	2.666

^{&#}x27;K(he) refers to the gas permeability of a rock sample measured using helium (He) gas in laboratory settings.

ROCK PHYSICS DIAGNOSTICS, MODELLING AND CALIBRATION

The rock physics modelling (RPM) feasibility plots confirm that sand, shale, and coal lithologies are clearly distinguishable based on their elastic responses. In particular, the crossplot of recorded P-velocity

 (V_P) versus bulk density (RHOB), colour-coded with volume of clay (VCLSM), reveals distinct lithological trends across the seven analysed wells (Figure 8).

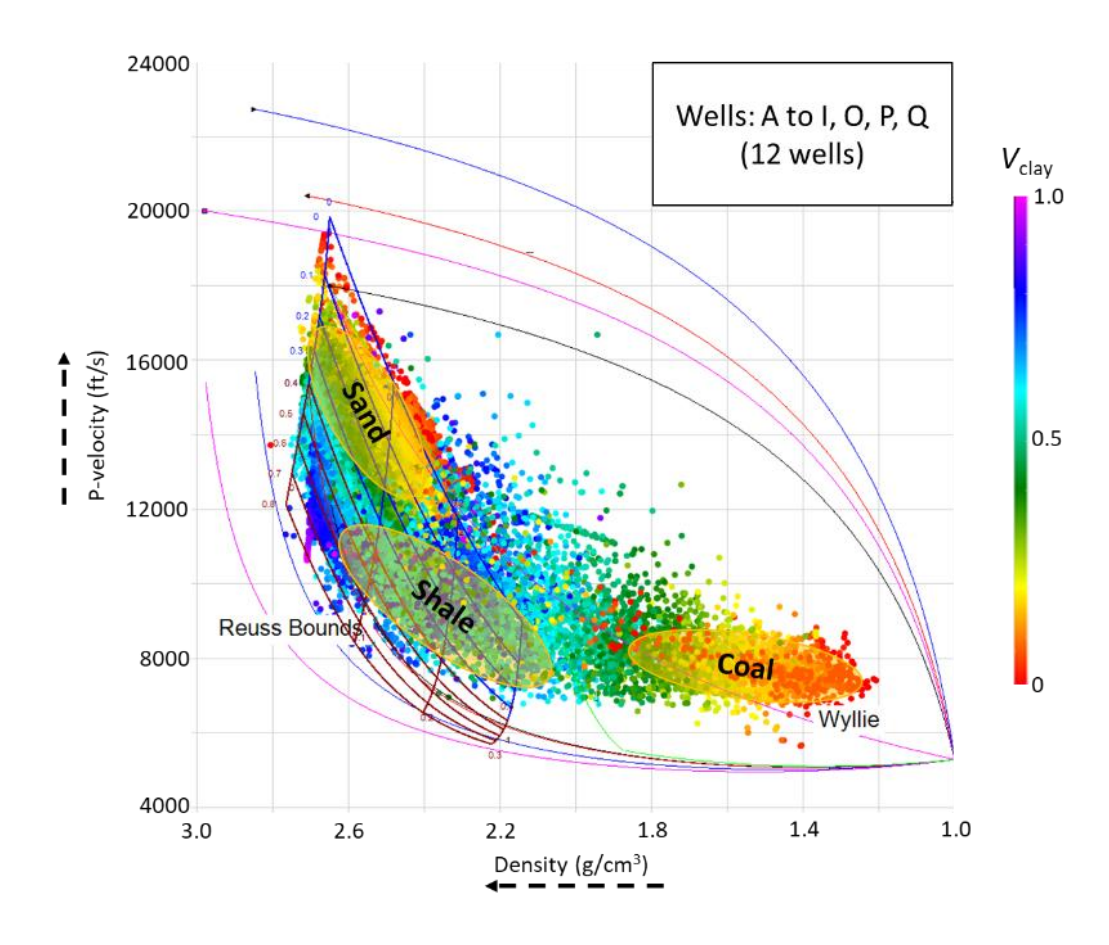


Figure 8: Crossplot between P-velocity (V_P) and bulk density (RHOB), colour-coded with VCLSM. The plot is overlaid with a bounds template to delineate lithofacies clusters, aiding in the identification of sand, shale, and mixed lithologies within the BCS section. (Mavko et al., 1998)

As a crucial step in the rock physics diagnostic process, we try and understand the behaviour of the raw data set by overlaying different rock physics templates with an objective to choose a template which honors the trend of the recorded data set and satisfies the log response against a particular depositional environment. The same exercise has been carried out in this study also (Figure 9). The diagnostic has been carried out using the approach of Odegaard and Avseth (2004).

These variations align well with known facies distributions, reinforcing the applicability of elastic attributes for lithofacies classification in the BCS interval. Analysis of all seven wells confirms that facies discrimination is achievable using both well log responses and P-velocity versus density crossplots. These tools consistently reveal distinct trends for sand, shale, and coal lithologies, supporting their application in elastic facies classification within the BCS formation (Figure 10).

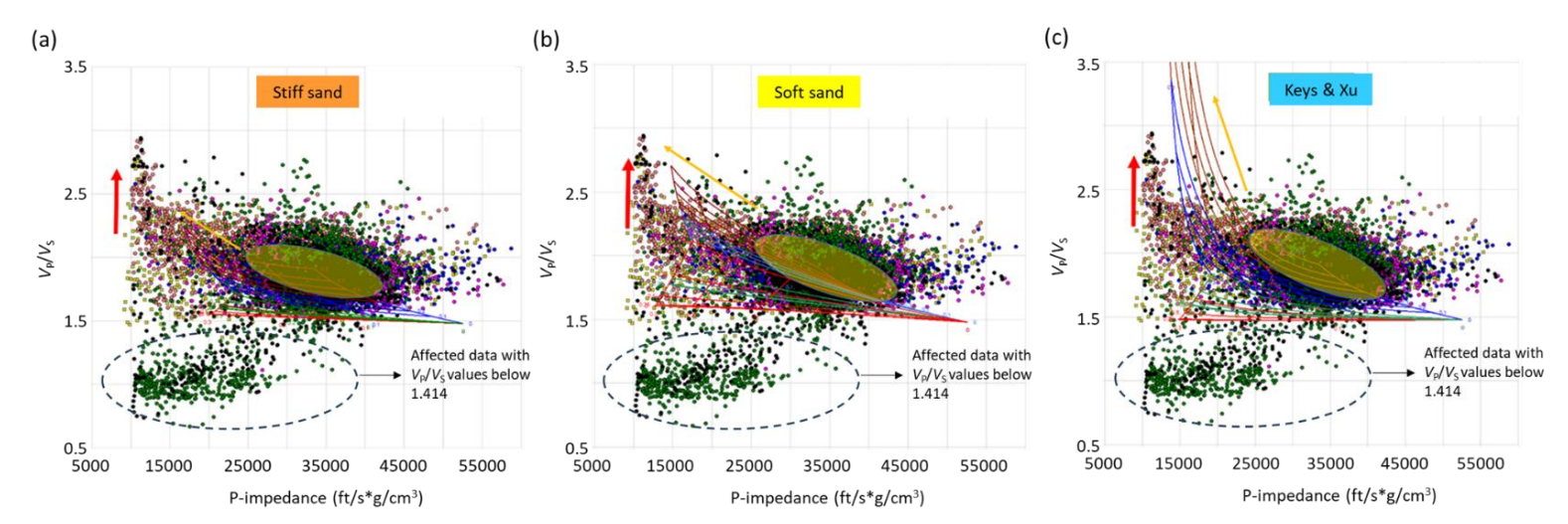


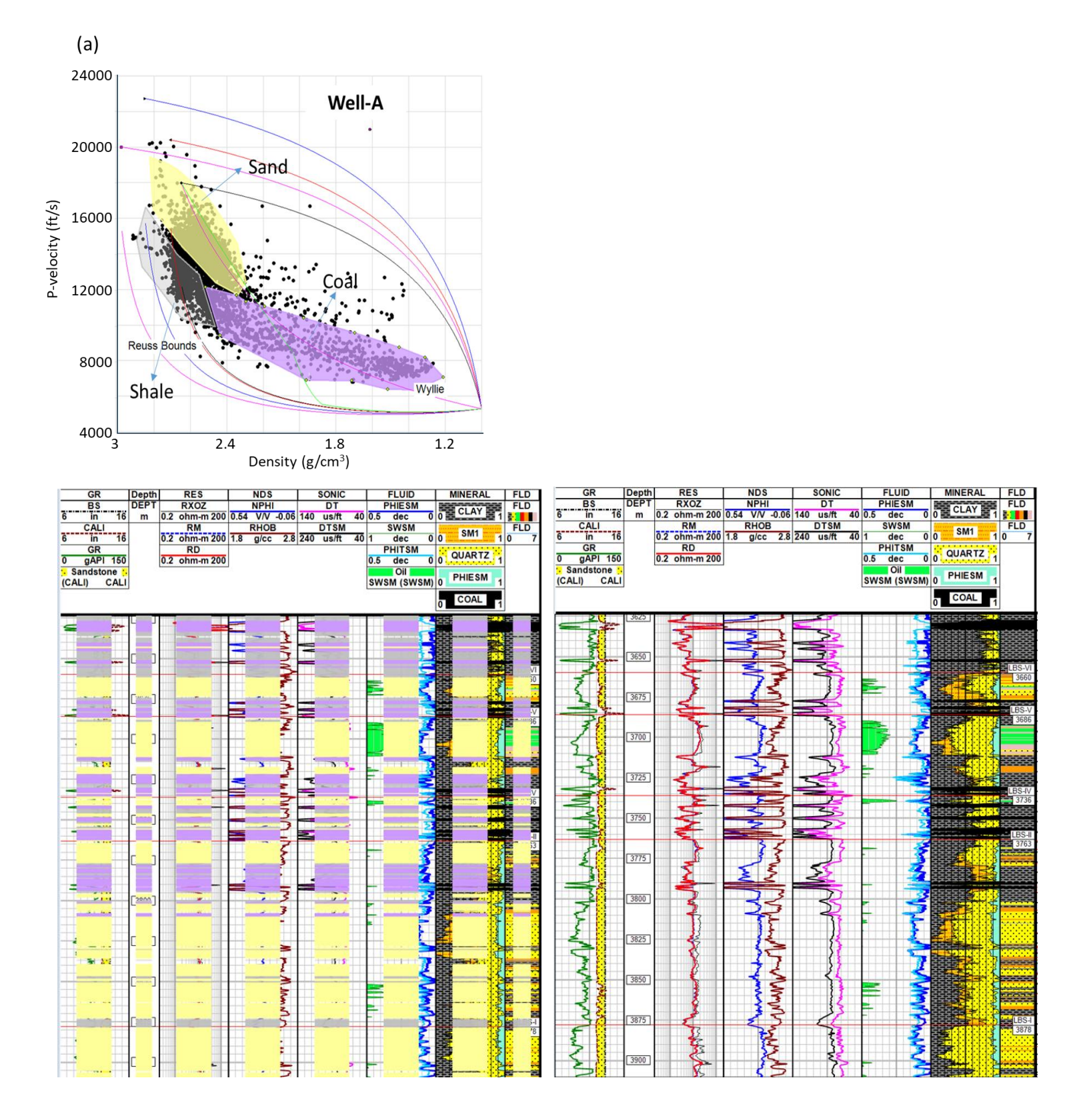
Figure 9: Crossplots between P-impedance and V_P/V_S derived from recorded log data, overlaid with rock physics templates for (a) stiff sand, (b) soft sand, and (c) Keys and Xu's rock physics model. These plots illustrate the elastic response of different lithofacies and demonstrate the effectiveness of rock physics modelling in distinguishing between sand, shale, and coal units within the BCS formation.

A notable feature observed in the crossplots is the distinct behaviour of carbonaceous shale intervals within the BCS section. These intervals typically occur within the inter-coal sequences, situated between two coal seams. The P-impedance and V_P/V_S associated with these carbonaceous shales tend to overlap with the response ranges of both coal and shale, making them a challenge to distinguish in isolation. Their elastic properties exhibit transitional characteristics, which emphasizes the importance of integrating geological context and petrophysical interpretation for accurate facies classification.

The crossplots of P-velocity versus total porosity shown in Figure 11 incorporate shale volume cutoffs to enhance lithological differentiation. A $V_{\rm shale}$ cutoff of 30% and RHOB>2.2 g/cm³ was used to classify sands, while a cutoff of 40% was applied for shales. Based on these thresholds, the plots clearly demonstrate distinct clustering of sand, shale, and coal facies, confirming that lithology can be reliably differentiated using a combination of porosity and elastic property

The Xu–White (1995) clay–sand mixing model employed in this study is derived from the Kuster and Toksöz (1974) effective medium theory and is supplemented by Brie's fluid mixing model (Brie et al., 1995) and Gassmann's (1951) fluid substitution model. This model allows for the differentiation of sand- and clay-related pores by assigning them distinct aspect ratios, thereby enhancing the accuracy of elastic property predictions in mixed lithologies.

Acoustic velocity was measured on 10 no. of core samples at varying pressure from 500 psi to 4000 psi. (Table 3) and their elastic constants were also computed (Table 4) . Average value of V_P and V_S at 500 psi & 4000 psi are 3421 m/s & 4673 m/s and 2039 m/s & 2487 m/s respectively for LBS Formation. It is observed that as the pressure increases the velocity increases (Figure 12). Based on the V_P – V_S relation measured at respective confining pressure, V_P – V_S transforms were also generated (Figure 13).



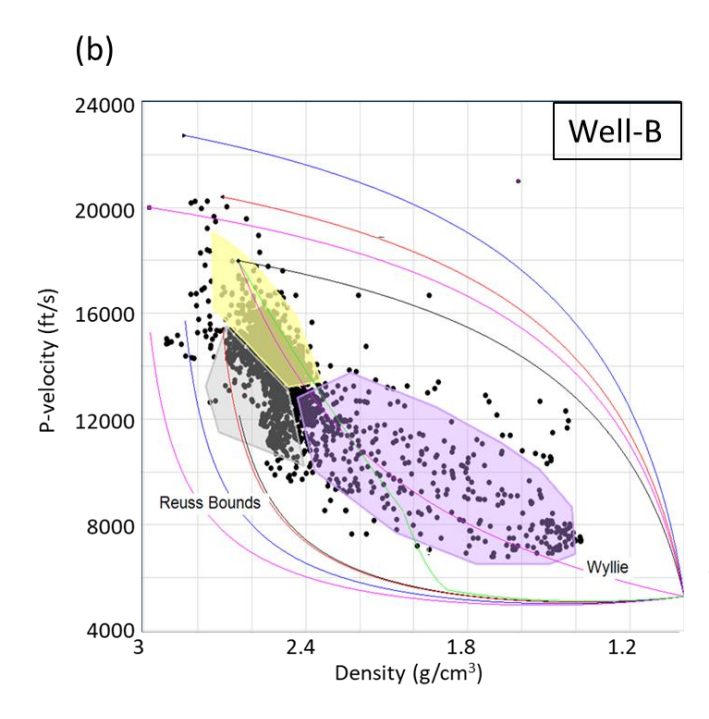
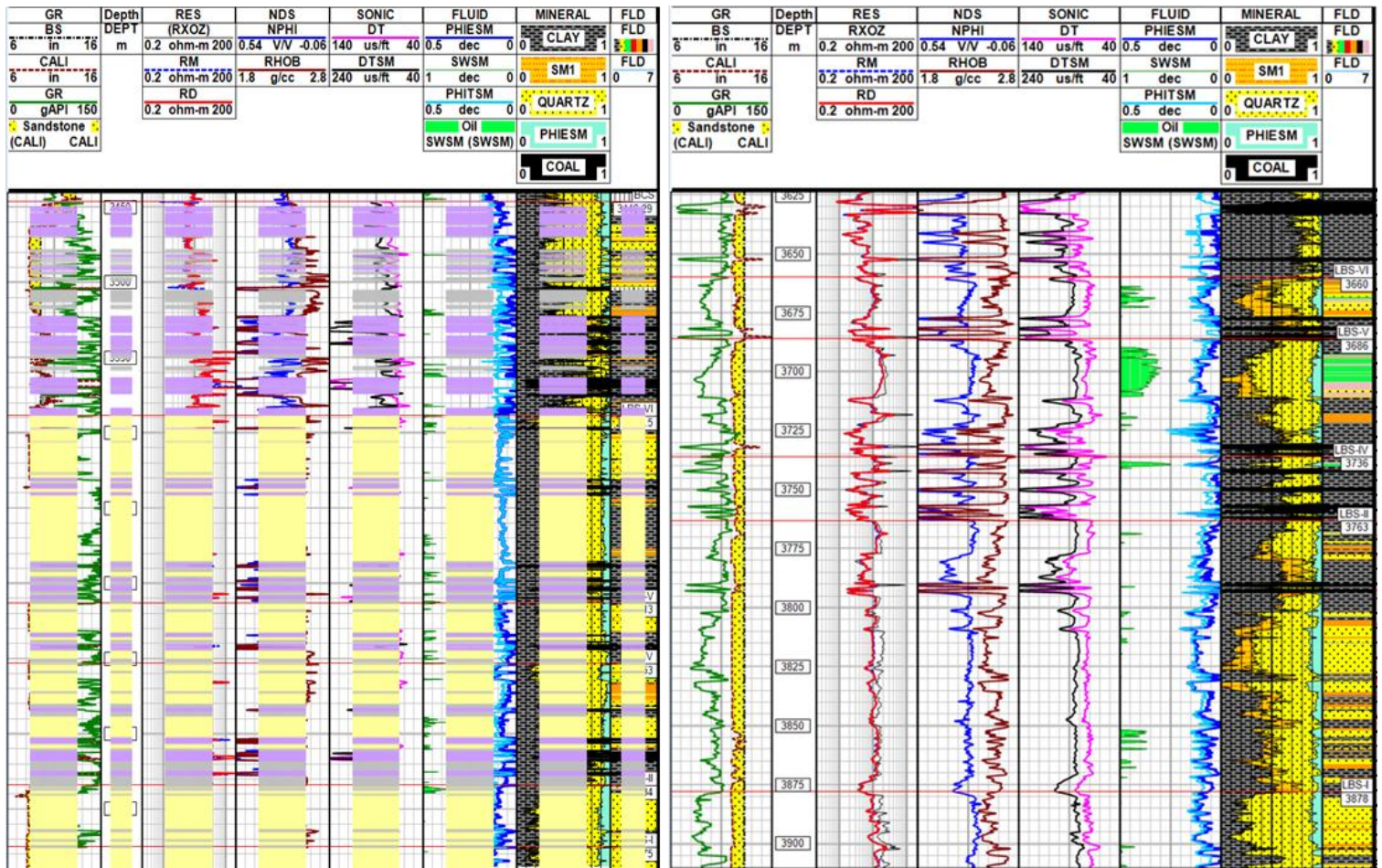


Figure 10: Interactive P-velocity versus density crossplot and paralog plot for (a) Well-A, and (b) Well B, highlighting the separation of sand, shale, and coal lithologies. The integration of petrophysical logs with elastic parameters allows for effective facies classification within the BCS section.



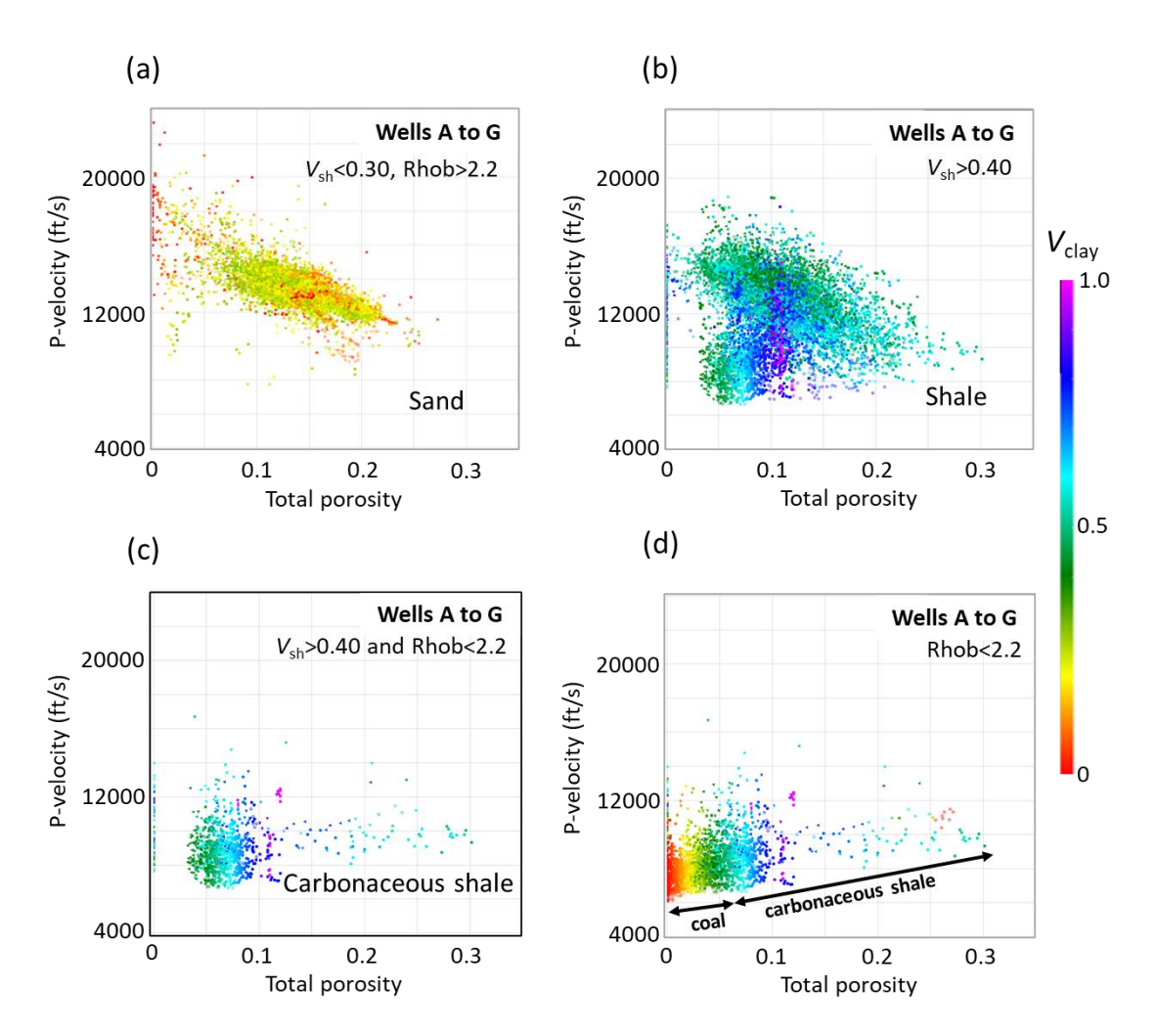


Figure 11: Crossplots of P-velocity versus total porosity, colour-coded with volume of clay. These plots demonstrate lithology separation across wells using porosity and velocity trends, supporting facies classification and elastic property modelling in the BCS section.

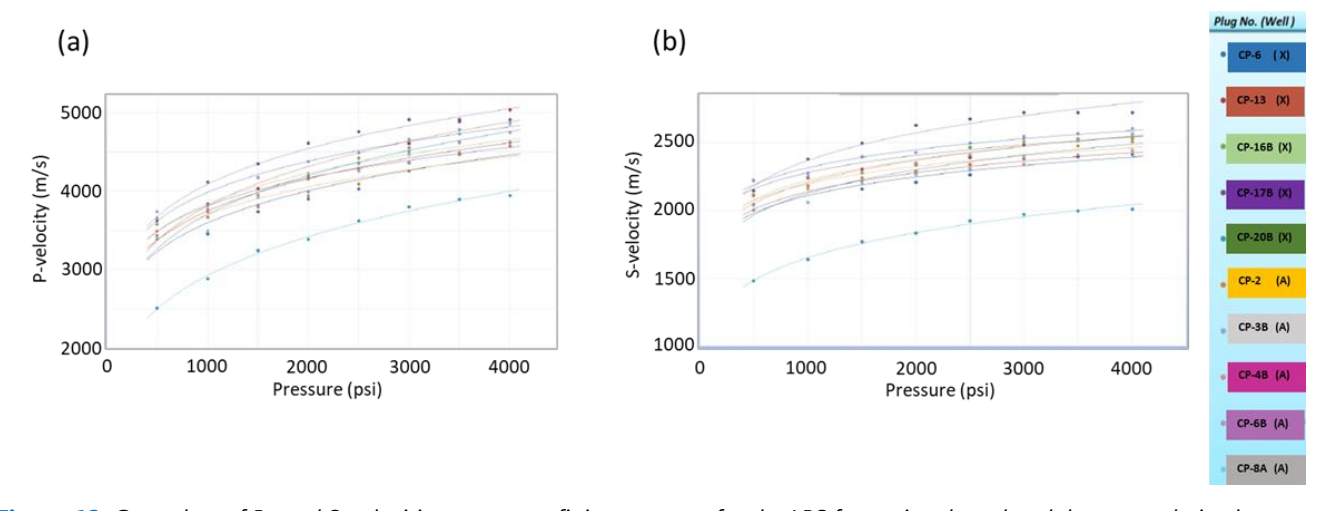


Figure 12: Crossplots of P- and S-velocities versus confining pressure for the LBS formation, based on laboratory-derived core measurements. These plots illustrate the pressure sensitivity of elastic wave velocities and support the calibration of rock physics models under near-reservoir stress conditions.

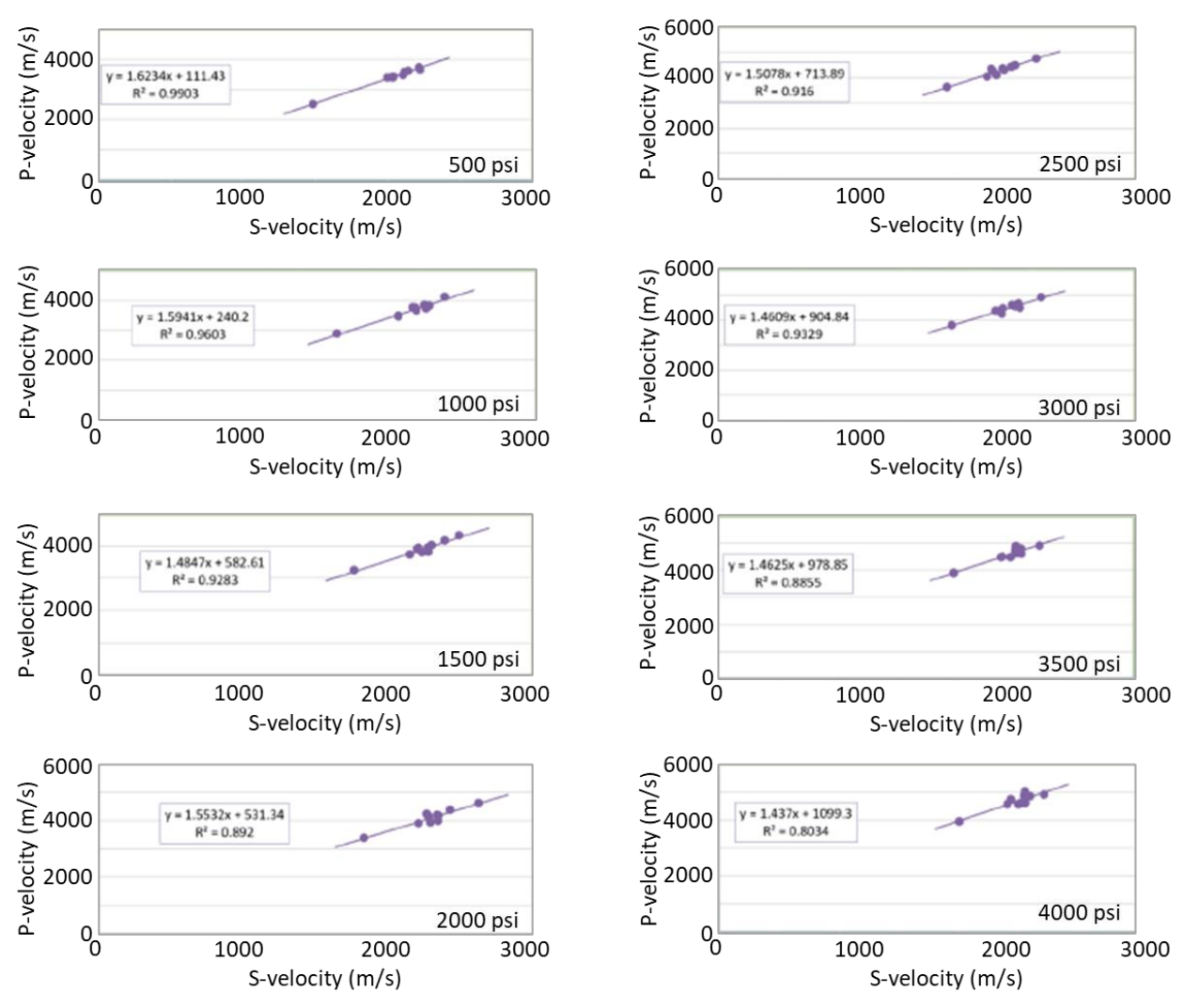


Figure 13: Crossplot of P-velocity versus S-velocity for the LBS Formation, based on laboratory measurements conducted at pressures ranging from 500 to 4000 psi. The plot demonstrates the linear correlation between P- and S-velocity under varying confining stress conditions, aiding in elastic calibration for rock physics modelling.

Table-3: P- and S-velocities (in m/s) at different pressures for LBS Sands

Plug No	At 500 psi		At 1000 psi		At 1500 psi		At 2000 psi		At 2500 psi		At 3000 psi		At 3500 psi		At 4000 psi	
	Vp	Vs	Vp	Vs	Vp	Vs	Vp	Vs	Vp	Vs	Vp	Vs	Vp	Vs	Vp	Vs
CP-2	3486	2105	3666	2181	3797	2238	3938	2287	4089	2337	4253	2389	4477	2473	4573	2502
CP-3B	3739	2215	3818	2272	4173	2393	4377	2425	4486	2492	4661	2527	4785	2564	4850	2601
CP-4B	3388	2000	3773	2156	3952	2213	4150	2274	4256	2306	4368	2338	4486	2406	4743	2441
CP-6B	3656	2222	3734	2250	3815	2279	3989	2340	4280	2404	4500	2543	4618	2562	4618	2562
CP-8A	3418	2034	3492	2060	3918	2201	4228	2263	4342	2295	4463	2398	4725	2510	4868	2550

S.No.	Plug No.	Poisso n's ratio	Young's modulus (E)*10^10 (Pa)	Bulk modulus (K)*10^10 (Pa)	Shear modulus (µ) *10^10 (Pa)	Lame's constant(λ) *10^9 (Pa)	Bulk volume Compressi bility (k)*10^11 (Pa-1)	Acoustic impedance (AI)*10^6 (kg/m²s)
1	CP-2	0.29	4.24	3.31	1.65	22.1	3.02	12.1
2	CP-3B	0.3	4.65	3.84	1.79	26.5	2.6	12.9
3	CP-4B	0.32	4.16	3.85	1.58	28	2.6	12.5
4	CP-6B	0.28	4.45	3.34	1.74	21.8	2.99	12.3
5	CP-8A	0.31	4.5	3.97	1.72	28.2	2.52	12.9

Table-4: Geomechanical Properties of plugs at 4000 psi

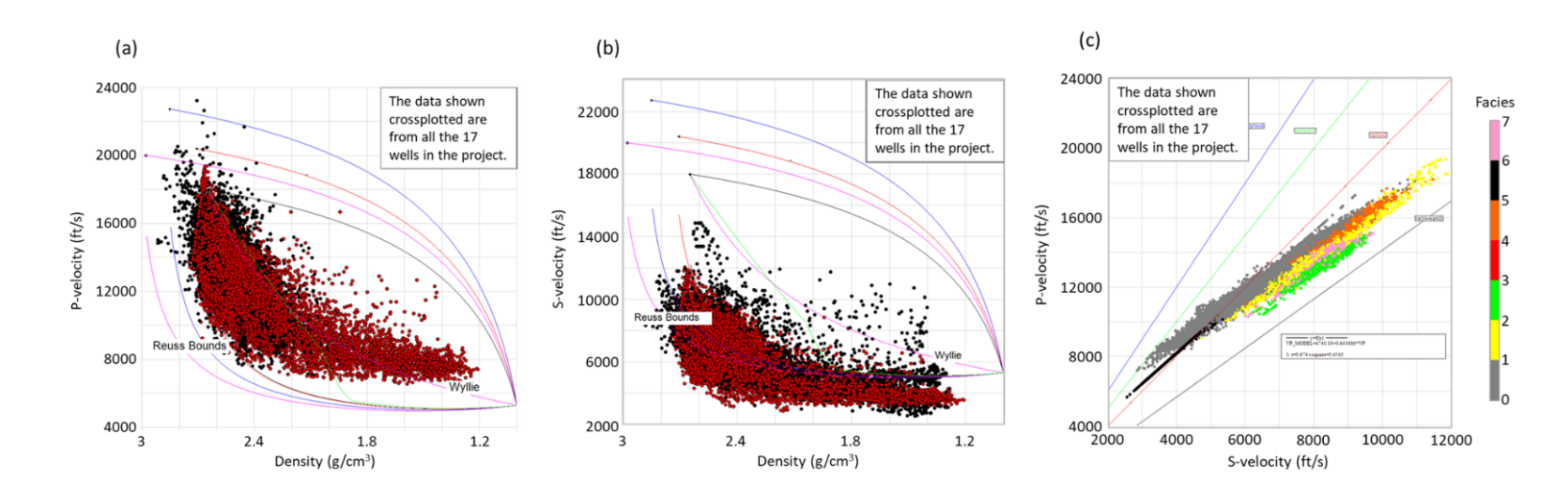


Figure 14: (a) and (b) Crossplot comparison of recorded (black) and modelled (red) P- and S-velocity versus density. The close alignment between measured and predicted curves validates the accuracy of the rock physics modelling and calibration workflow applied to the BCS section. (c) Crossplot of modelled P-velocity versus modelled S-velocity, color-coded with facies log.

DISCUSSION

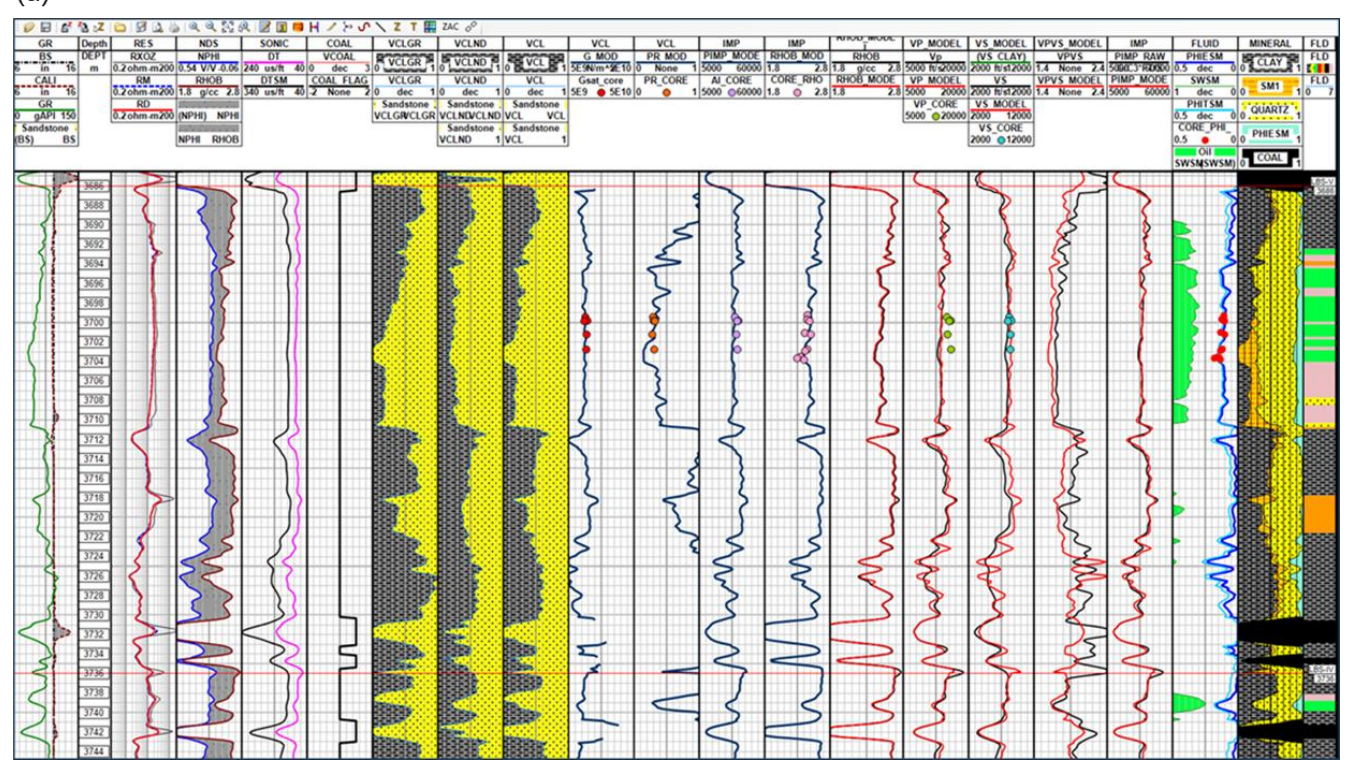
The reliability of the modelled results was validated by comparing modelled P- and S-velocities, V_P/V_S, density, and P-impedance with corresponding values measured on conventional core samples. These comparisons, shown on composite logs (Tracks 9-15 and 17 from the left in Figure 15a), indicate a strong correlation between recorded and modelled elastic parameters. Despite these geological complexities, the rock physics modelling was able to effectively capture the elastic behaviour of different facies. The shale intervals exhibited Pimpedance values ranging from 15,550 to 47,490 ft/s*g/cm³ and V_P/V_S typically between 1.72 and 2.50, with dominant values exceeding 1.75. Water-bearing sandstones showed P-impedance values from 23,865 to

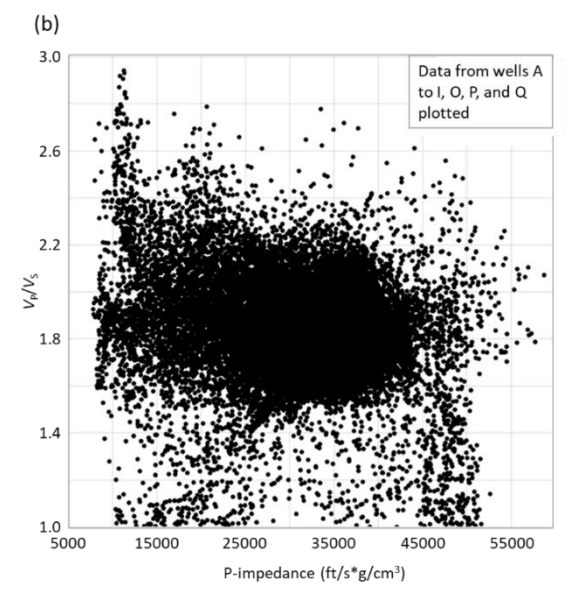
51,830 ft/s*g/cm³ and V_P/V_S from 1.60 to 1.86. The siltstone facies displayed similar elastic responses, with P-impedance values between 23,800 and 49,310 ft/s*g/cm³ and V_P/V_S from 1.62 to 1.85. Marginal hydrocarbon-bearing sandstones showed a slightly lower range of P-impedance values (24,110 to 40,000 ft/s*g/cm³) and V_P/V_S from 1.56 to 1.80, whereas distinct hydrocarbon-bearing reservoirs were identified with even lower P-impedance values (22,715 to 38,122 ft/s*g/cm³) and V_P/V_S between 1.53 and 1.72, with dominant values clustering in the 1.53–1.69 range. Coal intervals, by contrast, demonstrated significantly lower P-impedance values, ranging from 7,865 to 26,065 ft/s*g/cm³, and relatively high V_P/V_S from 1.94 to 2.17, allowing for their clear distinction from other facies. The

integration of core, log, and elastic modelling in this study has not only enabled accurate lithofacies discrimination but has also laid the groundwork for standardizing a reservoir characterization workflow applicable to future wells in the Kuargaon,

Lakwa-Lakhmani, Demulgaon, and Mahakuti Fields. This work reinforces the value of rock physics as a bridging tool between geology, petrophysics, and seismic interpretation in complex deltaic systems.

(a)





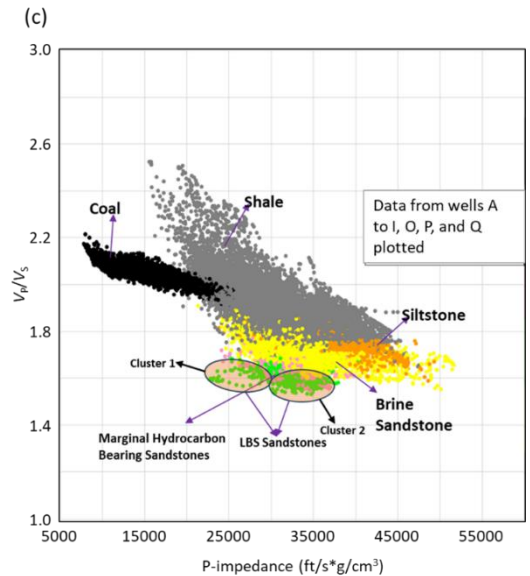




Figure 15: (a) The modelled outputs logs are shown from track 9 to track 16. The derived outputs are observed to have a good degree of matching with the core derived parameters. Track no 17 shows the computed porosity log, which is interpreted to be corroborating with the core derived porosity. Crossplots of P-impedance versus V_P/V_S , (b) recorded, and (c) modelled log data color-coded by facies log generated using. These plots highlight the separation of lithofacies—sand, shale, and coal—based on their elastic responses, further validating the rock physics model's capability in facies and fluid discrimination within the BCS formation. The legend for the facies log is shown in Figure 15(d).

CONCLUSIONS

Observations from conventional core data reveal that shale facies frequently contain siltstone stringers, and that ripped-up mudstone clasts are commonly embedded within the sandstone bodies representing a complex depositional environment that posed challenges for elastic property modelling. Notably, the Keys and Xu (2002) rock physics model proved highly effective discriminating in only lithofacies but also fluid types within the BCS sands, as illustrated in Figure 15. This model's ability to capture the mechanical and fluid-related variations in elastic properties highlights its applicability in deltaic, coal-rich environments such as the Upper Assam Shelf. The approach was successfully applied to characterize the LBS, despite the presence of borehole challenges, carbonaceous shales, and thinly interbedded coals. A standardized **RPM** workflow has been conceptualized through this study, which can be extended to future wells in the Kuargaon, Lakhmani, Demulgaon, and Mahkuti Fields. The workflow adopted can also prove to be useful in areas of similar geological setting globally where there are sands encapsulated between coal-shale-carbonaceous lithologies. Highquality shear logs were generated in the problematic borehole conditions using a combination of log conditioning, synthetic modelling, and template calibration. Water-bearing sandstones exhibited Pimpedance values ranging from 23,865 to 51,830 ft/s*q/cm³ and V_P/V_S ratios between 1.60 and 1.86. Marginal hydrocarbon-bearing sandstones showed slightly reduced P-impedance values, ranging from 24,110 to 40,000 ft/s*g/cm³, with V_P/V_S ratios between 1.56 and 1.80. In contrast, well-defined hydrocarbonbearing reservoirs were characterized by even lower P-impedance values (22,715 to 38,122 ft/s*g/cm³) and V_P/V_S ratios from 1.53 to 1.72, predominantly clustering in the 1.53–1.69 range. Moreover, we can also observe that the hydrocarbon bearing sandstones within LBS are of two types. One cluster has lower impedance and higher V_P/V_S values whereas another cluster is characterized by higher impedance and lower V_P/V_S values (Figure 15c). This information will prove to be beneficial in further classifying the LBS sands based on their elastic response. G

ACKNOWLEDGEMENTS

The authors would like to express their gratitude to Director (Exploration), ONGC, for providing the opportunity to undertake this work. They also sincerely acknowledge ED-COI, GEOPIC and Petrophysics Division, KDMIPE, ONGC, Dehradun for encouragement and support in publishing this work. Special thanks are extended to Head-INTEG, GEOPIC, Head-Petrophysics Group, INTEG, and the A&AA Basin Group, INTEG, GEOPIC, and Head KDMIPE for their valuable technical support and guidance throughout the study.

REFERENCES

Avseth, P., T. Mukerji, G. Mavko, and J. Dvorkin, 2010, Rock-physics diagnostics of depositional texture, diagenetic alterations, and reservoir heterogeneity in high-porosity siliciclastic sediments and rocks — A review of selected models and suggested workflows, Geophysics, **75**(5), A31–A47.

https://doi.org/10.1190/1.3483770

Azeem, T., Y. W. Chun, M. Lisa, P. Khalid, L. X. Qing, M. I. Ehsan, J. W. Munawar, and W. Xie, 2017. An integrated petrophysical and rock physics analysis to improve reservoir characterization of Cretaceous sand intervals in Middle Indus Basin, Pakistan J. of Geophys. and Engn., 14(2), 212–225. https://doi.org/10.1088/1742-2140/14/2/212

Brie, A., F. Pampuri, A. F. Marsala and O. Meazza, Shear sonic interpretation in gas-bearing sands, SPE Annual Technical Conference and Exhibition, 1995.

https://doi.org/10.2118/30595-MS

Chakrabarty, S., M. Shukla, and D. Gorai, 2022, Origin and significance of glauconites in a sequence stratigraphic perspective: Sylhet Formation, Assam and Assam–Arakan Basin, India, *J. Earth Syst. Sci*, **131**,142,1-24. https://doi.org/10.1007/s12040-022-01887-0

Gassmann, F., 1951, Uberdieelastizit at por oser medien: Vierteljahrsschrift der Naturforschenden Gesellschaft in Zurich, **96**,1–23.

Keys, R.G. and Xu, S.Y., 2002, An approximation for the Xu–White velocity model, Geophysics, **67**(5), 1406-1411. https://doi.org/10.1190/1.1512786

Mavko, G., T. Mukerji, and J. Dvorkin, 1998, The Rock Physics Handbook: Tools for Seismic Analysis in Porous Media, Cambridge Univ. Press.

Odegaard, E. and P. Avseth, 2004, Well log and seismic data analysis using rock physics templates, First Break, **22**(10) 37-43. https://doi.org/10.3997/1365-2397.2004017

APPENDIX-A

The basic equations used for computation of volume of clay, porosity and water saturation (deterministic approach) and which were used as quality control curves for statistical mineral modelling are given below.

Volume of shale (V_{sh}): The volume of shale was estimated using both linear and non-linear methodologies. The linear approach is based on the Index Gamma Ray (IGR) method, while non-linear corrections were applied using established empirical models, including:

- Larionov (1969) for older rock formations
- Stieber (1970) accounts for laminated shale effects

• Clavier et al. (1971) – suited for clean to moderately shaly sands

$$I_{GR} = (GR_{log} - GR_{min}/GR_{max} - GR_{min}) \text{ and } I_{GR} = V_{sh}$$
 (7)

$$V_{sh(Larionov old)} = 0.33(2^{(2*IGR)} - 1)$$
 (8)

$$V_{sh(Steiber)} = I_{GR}/(3-2*I_{GR})$$
 (9)

$$V_{sh(Clavier)} = 1.7 (\sqrt{3.38 - (I_{GR} + 0.7)^2})$$
 (10)

Porosity: The initial step in porosity evaluation involved the generation of a density-derived porosity curve, using a core derived matrix density of 2.664 g/cc representing quartz, as the dominant matrix mineral in the formation (average matrix density computed from the core results, Table-1) and the recorded bulk density (RHOB) log. The density porosity (ϕ_d) was calculated using the standard equation:

This is given as
$$\Phi_d = (\rho_{\text{matrix}} - \rho_{\text{log}})/(\rho_{\text{matrix}} - \rho_{\text{fluid}})$$
 (11)

 ρ_{fluid} is taken as density of water/brine which is almost 1-1.03g/cc. The corrected porosities were computed using the following standard equations:

$$\Phi_{\text{nc}} = \Phi_{\text{n}} - V_{\text{sh}}^* \Phi_{\text{nsh}} \tag{12}$$

$$\Phi_{dc} = \Phi_{d^-} V_{sh}^* \Phi_{dsh} \tag{13}$$

Where Φ_{nc} and Φ_{dc} are shale corrected neutron and density porosities, Φ_{nsh} and Φ_{dsh} are neutron and density porosities of the shale respectively. V_{sh} is the volume of shale computed from the combined method.

Water Saturation: Water saturation (S_w) was computed using the Indonesian equation, which is well-suited for evaluating shaly sandstone reservoirs such as the BCS sands. The equation can be written as

$$S_{w}^{n} = [(R_{w}/\Phi^{m^{*}}R_{t})^{1/2} + (V_{s}h^{1-V_{s}h}/R_{sh})^{1/2}]^{2}$$
(14)

where S_w is the water saturation, n is the saturation exponent, R_w is the resistivity of the formation water, R_t is the true resistivity of the formation and V_{sh} denotes the final volume of shale computed through the combined methods.

BIOGRAPHIES



Jayendra Nath Chakraborty received a master's degree in applied geophysics from IIT Bombay in 2009. He began his career with the Directorate General of Hydrocarbons, Noida, and later worked as a QC geophysicist and seismic interpreter at Hindustan Oil Exploration Company (2011–2013), followed by a brief stint at Cairn India Ltd. He joined ONGC in 2013, serving as a wireline logging engineer in the western offshore and Kutch-Saurashtra Basin, conducting both open and cased hole operations. In 2016, he moved to Tripura Asset, Agartala, where he provided operational petrophysics support, carried out real-time log data monitoring, and formation evaluation, in addition to planned workover programmes. Since 2021, he has been based at GEOPIC, ONGC's R&D center in Dehradun, contributing to reservoir characterization, geocellular modeling, seismic petrophysics, and machine learning workflows. Jayendra has been conferred with Asset Award for "exemplary performance for identification of new gas reserves in Baramura Field, Tripura Asset".

Jayendra brings over a decade of experience across exploration and development geoscience functions. He is a petrophysics enthusiast and has a deep love for music.



HOI, GEOPIC (2020).

Manoj Kumar received an M.Tech. degree in applied geophysics from the Indian Institute of Technology, Roorkee in 2008, and began his career at ONGC the same year as a geophysicist (wells) at Nazira, Assam Asset. During his tenure there, he performed cased-hole wireline logging and production logging operations. In 2012, he transitioned to the Frontier Basin, Dehradun, where his role focused on monitoring logging field operations and log data management. Since 2014, he has been contributing at GEOPIC, Dehradun, with core expertise in petrophysical evaluation, rockphysics modeling of clastic and carbonate reservoirs, and geomechanical studies.

He has received several accolades for his professional contributions, including a Group Award from the Director (Exploration) in 2003 for exemplary exploration efforts, and Group Merit Awards from the ED-Asset Manager, Assam (2009), Basin Manager, Frontier Basin (2013), CMD (2018), and ED-



Debashree Paul is a petrophysicist with an M.Sc. Tech degree in applied geophysics from IIT, ISM, Dhanbad, with nearly 19 years of experience in the oil and gas industry. Her core expertise is in clastic reservoirs, with extensive work carried out in both eastern and western onshore basins of India. She has carried out a number of high-value studies integrating both log and core petrophysical data for reservoir estimation in unconventional reservoirs. Her portfolio also includes specialized projects focused on fracture identification and porosity determination in basement and basaltic trap sections, supporting both hydrocarbon exploration and carbon capture utilization and storage (CCUS) initiatives in India. Additionally, she has wide experience in doing 1D-Mechanical Earth Modelling (MEM) and perforation optimization for hydro-fracture simulation studies, particularly in the western onshore basin.



Sunil Kumar Singh is an exploration geoscientist with more than 25 years of experience in the E&P industry. He received his M.Sc. (Tech.) in geophysics from Banaras Hindu University, Varanasi. Also, he received a Ph.D. degree from Osmania University, Hyderabad. He has published/ presented several papers at national and international conferences. His key area of interest is seismic reservoir characterization.